Computer Physics Communications 127 (2000) 59–70

Computer Physics Communications

www.elsevier.nl/locate/cpc

Electromagnetic gyrokinetic-ion drift-fluid-electron hybrid simulation

Scott E. Parker *, Yang Chen, Charlson C. Kim

Center for Integrated Plasma Studies, Department of Physics, University of Colorado at Boulder, Boulder, CO 80309, USA

Abstract

Progress on gyrokinetic-ion drift-fluid-electron hybrid simulation is reported. Simulation results are shown from a three-dimensional toroidal electromagnetic simulation using field-line-following coordinates. It is found that for $\beta \gtrsim 1.5\%$ there is strong destabilization of Alfvénic ion-temperature-gradient (ITG) driven instabilities. Nonlinear results show a corresponding increase in the the ion heat flux. Secondly, we report very good parallel performance and near perfect scalability was shown on the Cray T3E and SGI O2K using a one-dimensional domain decomposition and digital filtering to handle the shift at the boundary along the magnetic field-line due to toroidal boundary conditions. Finally, we report recent results in the electrostatic limit, which explore a scheme to reduce the heat flux by adding a ripple to the ion temperature profile. Both self-generated and equilibrium E_r shear flows are included for the first time. It may be possible to achieve similar results experimentally using ion cyclotron resonance heating.

PACS: 52.35.Ra; 52.35.Qz; 52.55.Fa; 52.65.Tt

1. Introduction

There has been enormous progress in the area of gyrokinetic simulation of tokamak plasma ion-temperature-gradient (ITG) driven turbulence in the past few years. Progress has included realistic dimensionality and geometry, large plasma volumes, and beginning comparisons with experiment [1–4]. These simulations are fast-becoming a valued tool in improved understanding of anomalous transport. As our understanding becomes better, it may be possible to improve plasma confinement. Shear flow stabilization is one such example [5–9]. Here, we discuss recent progress on a possible scheme to reduce heat transport by slightly rippling the temperature profile.

Most of the glowing success of gyrokinetic turbulence simulation has been made in the electrostatic limit. Progress with electromagnetic simulations, not surprisingly, has been slower. This is partially because of the increased complexity. But, more importantly, there are issues relating to electron free streaming. The passing electrons carry the bulk of the parallel current, so the electron transit motion must be resolved. In addition, the discrete simulation particles (especially the fast electrons) Cherenkov emit, and these fluctuations are weakly damped since $\frac{\omega}{k_\parallel v_{te}} \ll 1$ for the highest frequency normal mode in the system, the shear Alfvén wave. This is the so-called "electron free-streaming noise" problem in electromagnetic gyrokinetic simulation. In addition, there

* Corresponding author. E-mail: scott.parker@colorado.edu.

0010-4655/00/$ – see front matter
PII: S0010-4655(00)00027-8

is an accuracy condition $k_\parallel v \Delta t < 1$ for the fast electrons limiting electromagnetic simulations to a small timestep or compressed ion-to-electron mass ratio.

Even with these limitations, there has been significant progress on electromagnetics over the past few years in the small β limit using various techniques, including using generalized Ohm's laws, canonical momentum formulations, and semi-implicit methods [10–13]. Here, we take the simplest path towards getting the electron parallel current, and hence, low β electromagnetics. We treat the electrons as a zero-inertia drift-fluid. This circumvents the electron free-streaming noise and any restrictions on $k_\parallel v_{\mathrm{te}} \Delta t$. There has been recent progress using a similar model for electrons in electromagnetic gyrofluid simulations [14,15].

The gyrokinetic equations are derived using a perturbative expansion in the following small quantities $\epsilon \sim \omega/\Omega_{\mathrm{i}} \sim e\delta\phi/T_{\mathrm{e}} \sim \delta n/n \sim k_\parallel/k_\perp \sim \rho_{\mathrm{i}}/L \sim \epsilon$, where ϵ is small. L is the equilibrium gradient scale length. The Vlasov–Maxwell system is then averaged over the fast gyro-motion, retaining finite Larmor radius (FLR) effects. Nonlinear equations were formulated in the 1980's [16–21] and it is now fairly well accepted that the gyrokinetic equations are a good starting point for low-frequency tokamak plasma physics. The gyrokinetic equation is very similar to the more basic Vlasov equation, but in a reduced five-dimensional phase space for particle guiding centers

$$\frac{\partial f}{\partial t} + \dot{\mathbf{z}} \cdot \frac{\partial f}{\partial \mathbf{z}} = 0, \tag{1}$$

where $\mathbf{z} = (\mathbf{R}, v_\parallel, \mu)$, and $\mathbf{R}$ is the guiding center position and $v_\parallel$ is the velocity along the magnetic field. The equation of motion for a guiding center defines $\dot{\mathbf{z}}$ and it includes gyro-averaging of field quantities. $\mu \equiv m v_\perp^2/(2B)$ is time independent.

Our approach to solving Eq. (1) is to first write the total distribution function in terms of the equilibrium and perturbed parts $f(\mathbf{z}, t) = f_0(\mathbf{z}) + \delta f(\mathbf{z}, t)$. $\dot{\mathbf{z}}$ is expanded into equilibrium and perturbed parts as well $\dot{\mathbf{z}} = \dot{\mathbf{z}}^0 + \dot{\mathbf{z}}^1$. $f_0(\mathbf{z})$ is an equilibrium distribution which satisfies $\dot{\mathbf{z}}^0 \cdot \partial_{\mathbf{z}} f_0(\mathbf{z}) = 0$. The equation for δf is

$$\partial_t \delta f + \dot{\mathbf{z}} \cdot \partial_{\mathbf{z}} \delta f = -\dot{\mathbf{z}}^1 \cdot \partial_{\mathbf{z}} f_0. \tag{2}$$

This equation is solved by following characteristics along particle trajectories. We evolve the particle weights w_i, defined as [22] $w_i \equiv \frac{\delta f}{f}|_{\mathbf{z}=\mathbf{z}_i,t}$. These weights are evolved in time and are deposited on the grid.

Using the toroidal electromagnetic equations in the low β limit [19,20], neglecting $\delta \mathbf{B}_\parallel$, the equilibrium and perturbed particle trajectories are

$$\dot{\mathbf{R}}^0 = \frac{1}{B^*}\left\{ v_\parallel \mathbf{B}^{*0} + \frac{c}{e}\hat{\mathbf{b}} \times \mu \nabla B^0 \right\}, \tag{3}$$

$$\dot{v}_\parallel^0 = -\frac{1}{B^*}\left\{ \mathbf{B}^{*0} \cdot \frac{\mu}{m} \nabla B^0 \right\}, \tag{4}$$

$$\dot{\mathbf{R}}^1 = \frac{1}{B^*}\left\{ v_\parallel \delta \bar{\mathbf{B}}_\perp + c\hat{\mathbf{b}} \times \nabla \delta \bar{\phi} \right\}, \tag{5}$$

$$\dot{v}_\parallel^1 = \frac{1}{B^*}\left\{ \mathbf{B}^{*0} \cdot \frac{e}{m} \overline{E}_\parallel \hat{\mathbf{b}} + \delta \bar{\mathbf{B}}_\perp \cdot \frac{\mu}{m} \nabla B^0 \right\}, \tag{6}$$

where $\hat{\mathbf{b}}$ is the direction of the equilibrium magnetic field, $\hat{\mathbf{b}} = \mathbf{B}_0/B$ with $B = |B| \simeq B_0$. Also,

$$\mathbf{B}^* = \mathbf{B}^0 + \delta \bar{\mathbf{B}}_\perp + \frac{mc}{e} u \nabla \times \hat{\mathbf{b}}, \qquad B^* = \hat{\mathbf{b}} \cdot \mathbf{B}^*,$$

and

$$\mathbf{B}^{*0} = \mathbf{B}^0 + \frac{mc}{e} u \nabla \times \hat{\mathbf{b}}.$$

The bar represents gyroaveraged quantities, e.g.,

$$\delta \bar{\phi} = \frac{1}{2\pi} \int \delta\phi(\mathbf{R} + \rho)\, \mathrm{d}\theta.$$

The quasi-neutrality condition [17] in Fourier space is

$$-\frac{\rho_s^2}{\rho_i^2\lambda_D^2}\big[1-\Gamma_0(b)\big]\phi = -4\pi e(\delta\bar{n}_i - \delta n_e), \tag{7}$$

where $\delta n = (n - n_0)/n_0$, $\delta\bar{n}_i$ is the gyro-phase-averaged ion density, $b = (k_\perp\rho_i)^2$, $\rho_s^2 \equiv T_e/T_i\rho_i^2$, $\lambda_D \equiv \sqrt{T_e/(4\pi n_0 e^2)}$, and higher order terms have been neglected in Eq. (7). In the small b limit Eq. (7) reduces to $(\rho_s/\lambda_D)^2\nabla_\perp^2\phi = -4\pi e(\delta\bar{n}_i - \delta n_e)$. To avoid any confusion, throughout this paper $T_i = T_e$ and $\rho_i = \rho_s$.

The electromagnetic part of the field quantities are obtained from Ampere's law

$$\nabla_\perp^2 A_\parallel = -\frac{4\pi}{c}(\bar{J}_{\parallel i} + J_{\parallel e}), \tag{8}$$

along with the following definitions

$$\delta\mathbf{B}_\perp = \nabla A_\parallel \times \hat{\mathbf{b}}, \tag{9}$$

$$E_\parallel = -\hat{\mathbf{b}}\cdot\nabla\phi - \frac{1}{c}\partial_t A_\parallel. \tag{10}$$

The gyroaveraged perturbed ion density is

$$\delta\bar{n}_i = \int \delta f\,\delta(\mathbf{R}+\rho-\mathbf{x})\,\mathrm{d}\mathbf{R}\,\mathrm{d}^3v,$$

and the gyroaveraged perturbed ion current is

$$\bar{J}_i = \int v_\parallel \delta f\,\delta(\mathbf{R}+\rho-\mathbf{x})\mathrm{d}\mathbf{R}\,\mathrm{d}^3v.$$

Gyroaveraging is done using the 4-point averaging scheme [23].

Section 4 will discuss the electromagnetic drift-fluid electron model extension. In Section 5 we take the electrostatic limit and assume an adiabatic electron response $\delta n_e/n_0 = e(\delta\phi - \langle\delta\phi\rangle)/T_e$ [24,25], this is the typical limit for core turbulence simulations.

The organization of the paper follows: In Section 2, we will discuss the toroidal field-line-following coordinate system and computational domain. Section 3, will discuss the parallel algorithms and performance on the Cray T3E and SGI O2K. In Section 4 we describe the electromagnetic drift-fluid electron model with results showing fairly strong destabilization at larger values of $\beta \gtrsim 1.5\%$. Finally, in Section 5 we describe recent results that show how a small ripple in the equilibrium temperature profile can reduce the heat transport. These results presented here include an equilibrium radial electric field which was previously neglected [26] and is an important effect.

2. Field-line following coordinates

In this section, a brief overview of the simulation geometry is given. The simulation domain is a magnetic flux tube and contains the minimum plasma volume necessary to model high-n drift-type micro-instabilities by utilizing the alignment of the long twisted eddies, i.e. $k_\parallel \ll k_\perp$ [27,25]. The field-line-following coordinates used in this simulation are [25]

$$x = r - r_0, \qquad y = \frac{r_0}{q_0}\big(q(r)\theta - \psi\big), \qquad z = Rq_0\theta, \tag{11}$$

where r is the minor radius, θ is the poloidal angle, ψ is the toroidal angle, q is the safety factor, $q_0 = q(r_0)$, and $R = R_0$ is the major radius. The width of the box in the radial direction is assumed small compared to r_0, $\mathrm{d}q/\mathrm{d}r$ is assumed constant. A zero β unshifted circular magnetic equilibrium and small r_0/R are also assumed. The domain is rectilinear in the field-line-following coordinates and is taken to be periodic in x and y. At the ends of

the box $z = \pm Rq_0\pi$ periodicity in θ and ψ is enforced [25]. These boundary conditions may be justified if the box size is larger than the correlation length in the perpendicular directions. The particle equations of motion used in the simulation are obtained by transforming Hamiltonian guiding center equations [28] to the field-line-following coordinates keeping only terms first order in r/R. This twisted nonorthogonal coordinate system has the following "nice" gradient operators:

$$\hat{\mathbf{b}} \cdot \nabla f = \frac{\partial f}{\partial z}, \tag{12}$$

$$(\hat{b} \times \nabla \delta\phi) \cdot \nabla f = \frac{\partial \delta\phi}{\partial y}\frac{\partial f}{\partial x} - \frac{\partial \delta\phi}{\partial x}\frac{\partial f}{\partial y}, \tag{13}$$

$$\nabla_\perp^2 \delta\phi = \frac{\partial^2 \delta\phi}{\partial x^2} + (1 + s^2 z^2)\frac{\partial^2 \delta\phi}{\partial y^2} + 2sz\frac{\partial^2 \delta\phi}{\partial x \partial y}, \tag{14}$$

to leading order, where $s = 1/L_s = r_0 q'/Rq^2$. The variation of the ρ_i along the magnetic field line can be taken into account in quasi-neutrality equation, Eq. (4), using $\rho_\mathrm{i}^2 = 1 + 2(r_0/R)\cos\theta$, so that

$$k_\perp^2 \rho_\mathrm{i}^2 = \left[k_x^2 + (1 + s^2 z^2)k_y^2 + 2szk_x k_y\right]\left[1 + 2(r_0/R)\cos\theta\right]. \tag{15}$$

3. Parallel performance

In this section we briefly outline the algorithm and report timings and scaling studies. A one-dimensional domain decomposition [29] is used along the magnetic field line (in the z-direction). Particles are sorted so that they are located on the processor assigned to their particular local z-grid cell. The system is not periodic in the z-direction because there is a shift in y to enforce periodicity in the toroidal coordinates (r, θ, ψ). This prevents using a fast Fourier transform in z. The field solve is done spectrally in (x, y) at every z-grid cell. Digital smoothing is applied in the z-direction. Even with these complications, performance is quite good with near-perfect scalability.

Fig. 1 shows a very simple scaling study using a 64^3 grid with 8 particles per cell run on 4, 8, 16, 32, and 64 processors. In this section, all timings are done in the electrostatic limit. We expect the electromagnetic model to

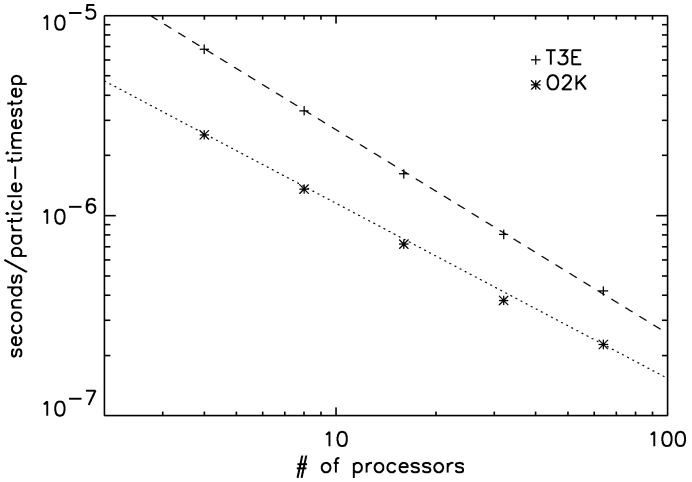

Fig. 1. Simple scaling study showing computing time scales as the inverse of the number of processors for a fixed problem size. $64 \times 64 \times 64$ grid with 8 particles per grid cell.

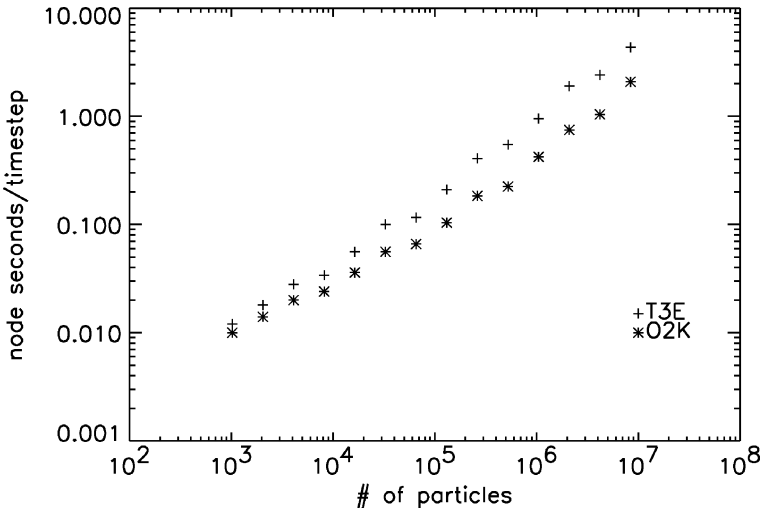

Fig. 2. T3E and O2K timings for different numbers of processors and problem sizes (wall clock in seconds/step, speed in μs-PE/particle-step). See Table 1 for data details.

Table 1
T3E and O2K timings for different numbers of processors and problem sizes (wall clock in seconds/step, speed in μs-PE/particle-step)

# part	Grid size	Part./cell	# PE	Wall-clock		Speed	
				T3E	O2K	T3E	O2K
2^{10}	$8 \times 8 \times 4$	4	4	0.012	0.010	46.9	49.1
2^{11}	$8 \times 8 \times 4$	8	4	0.018	0.014	35.2	27.3
2^{12}	$8 \times 8 \times 4$	16	4	0.028	0.020	27.3	19.5
2^{13}	$16 \times 16 \times 8$	4	8	0.034	0.024	33.2	23.4
2^{14}	$16 \times 16 \times 8$	8	8	0.056	0.036	27.3	17.6
2^{15}	$16 \times 16 \times 8$	16	8	0.100	0.056	24.4	13.7
2^{16}	$32 \times 32 \times 16$	4	16	0.116	0.066	28.3	16.1
2^{17}	$32 \times 32 \times 16$	8	16	0.210	0.104	25.6	12.7
2^{18}	$32 \times 32 \times 16$	16	16	0.408	0.184	24.9	11.2
2^{19}	$64 \times 64 \times 32$	4	32	0.548	0.224	33.4	13.7
2^{20}	$64 \times 64 \times 32$	8	32	0.952	0.422	29.1	12.9
2^{21}	$64 \times 64 \times 32$	16	32	1.906	0.748	29.1	11.4
2^{22}	$128 \times 128 \times 64$	4	64	2.408	1.042	36.7	15.9
2^{23}	$128 \times 128 \times 64$	8	64	4.346	2.086	33.2	15.9
2^{23}	$128 \times 128 \times 64$	8	64	4.346	2.086	33.2	15.9
2^{24}	$128 \times 128 \times 64$	16	64	7.050	3.618	26.9	13.8

be approximately twice as slow because of added gather operations for $\delta B_\perp$ in the particle push, and ion-current deposition. Detailed timings of the electromagnetic model have not yet been made. For the T3E we find the total CPU time (essentially wall clock) scaling as $N_p^{-1.0}$, and for the O2K we find $N_p^{-0.9}$, where N_p is the number of processors. In addition, the O2K is approximately twice as fast per processor. Fig. 2 shows the total CPU time defined as: $\sum_{\text{all CPUs}}$ individual processor CPU time). This shows good scalability is maintained over a wide variety of problem sizes and processor number.

The current simulation is limited to at least one z-grid cell per processor. This means the granularity is tied to the number of grid cells. Practically, this is not too much of a disadvantage, since available processors and problem size has been well balanced. However, we are currently developing a new algorithm which splits particles up on a given z-grid cell, assigning them to different processors, allowing for more grid cells than processors. For symmetric-multiprocessor/distributed memory hybrid computers, care needs to taken so that particles on the same grid cell share memory. This algorithm will be reported on later. An alternate approach is to use a two-dimensional domain decomposition [30].

4. Drift-fluid electron model

We now discuss the drift-fluid model which is derived from moments of the drift kinetic equation neglecting the electron inertia. The primary goal is to obtain the electron parallel current for electromagnetic simulations, yet still avoid accuracy or stability constraints on $k_\parallel v_{te}\Delta t$, as well as electron free streaming noise that has plagued previous models [10,11]. This is similar in spirit to previous zero-electron-mass models [31–33], but here the fluid equations are derived from the drift-kinetic equation. This approach was first suggested in Ref. [34] and similar drift-fluid electron equations have been very successful in electromagnetic gyrofluid simulations [15]. This approach provides a natural extension of previous electrostatic turbulence simulations and includes effects of electron $E\times B$ flow and electron pressure gradient effects (e.g., ω_{*e}). There is still a restriction on $k_\parallel v_A\Delta t = k_\parallel c_s\Delta t/\sqrt{\beta}$, which requires a smaller time step (by $\sqrt{\beta}$) relative to previous electrostatic ITG simulations, where $v_A^2 = B^2/(4\pi m_i n_0)$.

We begin with the drift kinetic equation for the electrons

$$\partial_t(Bf) + \nabla\left\{(v_\parallel\tilde{\mathbf{b}} + \mathbf{v}_E + \mathbf{v}_D)Bf\right\} + \partial_{v_\parallel}\left\{\left(\frac{e}{m_e}E_\parallel - \frac{\mu}{m_e}\tilde{\mathbf{b}}\cdot\nabla B + v_\parallel\hat{\mathbf{b}}\cdot\nabla\hat{\mathbf{b}}\cdot\mathbf{v}_E\right)Bf\right\} = 0, \tag{16}$$

where

$$\mathbf{v}_E \equiv \frac{c}{B}\hat{\mathbf{b}}\times\nabla\delta\phi, \qquad \mathbf{v}_D \equiv \frac{m_e}{eB^3}\left(v_\parallel^2 + \frac{v_\perp^2}{2}\right)\mathbf{B}\times\nabla B,$$

and

$$\tilde{\mathbf{b}} = \hat{\mathbf{b}} + \frac{\delta\mathbf{B}_\perp}{B}.$$

Integrating Eq. (16) over velocity we obtain the continuity equation

$$\partial_t\delta n_e + \mathbf{v}_E\cdot\nabla(n_0+\delta n_e) + n_0\tilde{\mathbf{b}}\cdot\nabla\frac{u_{\parallel e}}{B} + \frac{1}{m_e\Omega_e B}\hat{\mathbf{b}}\times\nabla B\cdot\nabla(\delta P_{\perp,e} + \delta P_{\parallel,e}) + \frac{2n_0}{B^2}\hat{\mathbf{b}}\times\nabla B\cdot\nabla\delta\phi = 0, \tag{17}$$

where $\delta n_e = n_e - n_0$. Multiplying Eq. (16) by $v_\parallel$ and integrating over velocity, then assuming $m_e \approx 0$, but T_e finite we obtain

$$en_eE_\parallel = -\tilde{\mathbf{b}}\cdot\nabla P_\parallel. \tag{18}$$

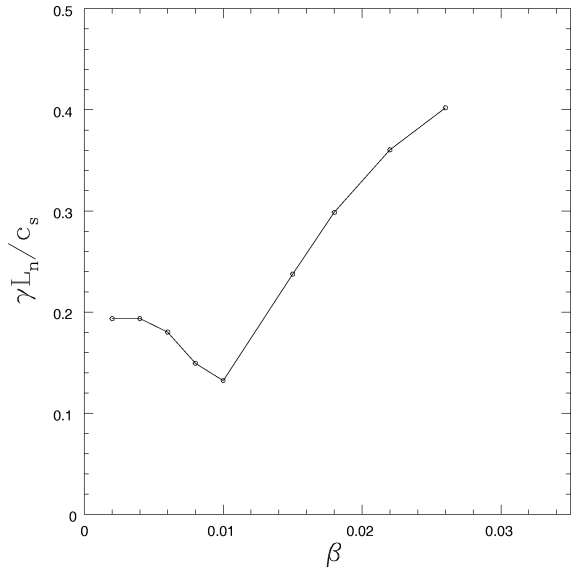

Fig. 3. Growth rate versus β for the DIII-D base case parameters. There is significant destabilization for $\beta \gtrsim 1.5\%$.

We can continue taking higher moments of Eq. (8), however, we first simply assume $\delta T_\parallel \approx 0$, hence

$$P_\parallel = P_{\parallel 0e} + \delta n_e T_{\parallel 0e}. \tag{19}$$

Eq. (18) can then be written as

$$e(n_0 + \delta n_e) E_\parallel = -\left(\hat{\mathbf{b}} + \frac{\delta \mathbf{B}_\perp}{B}\right) \cdot \nabla (P_{\parallel 0e} + \delta n_e T_{\parallel 0e}). \tag{20}$$

We also need to assume $\delta T_\perp \approx 0$ in Eq. (17). In the results shown below the electron equations Eqs. (17)–(20) are linearized, however, the ions are fully nonlinear. The $\delta n_e E_\parallel$ term in Eq. (20) would be neglected based on the $k_\parallel \ll k_\perp$ ordering. Another simple closure for $\delta T_\parallel$ has been suggested [14] using $\tilde{\mathbf{b}} \cdot \nabla (n_e T_{\parallel e}) = 0$. Work is in progress to compare this closure with Eq. (20). This model along with the gyrokinetic ions has been benchmarked with the shearless slab dispersion relation including full FLR and kinetic effects (using the Z-function) [35].

Fig. 3 shows the growth rate of the most unstable mode versus β for typical H-mode parameters. The ITG instability is unstable in the electrostatic limit. There is significant destabilization for $\beta \gtrsim 1.5\%$. The parameters are: $R/L_T = 6.9$, $R/L_n = 2.2$, $T_e/T_i = 1$, $r/R = 0.18$, $q = 1.4$, $\hat{s} \equiv r/q \cdot \mathrm{d}q/\mathrm{d}r = 0.78$. These are the "Cyclone Team DIII-D base case" parameters which is representative of a typical H-mode plasma (DIII-D Shot 81499), but assume a circular zero-beta large aspect ratio MHD equilibrium, no impurities, adiabatic electrons, and no fast ions, see Ref. [26] and references within, for further details. The numerical parameters are: 8 particles per cell, $64 \times 64 \times 32$ grid, with $\Delta x = \Delta y = \rho_s$, and a time step of $\Delta t c_s / L_T = 0.0345$. Fig. 4 shows the nonlinear heat flux versus time for the electrostatic case where $\beta = 0$ and an electromagnetic case with $\beta = 3\%$. There is a large increase in the heat flux for the large β case. The ideal ballooning limit is approximately

$$\beta < \frac{\sqrt{\frac{2}{3}s}}{q^2 \left(\frac{R}{L_T} + \frac{R}{L_n}\right)}$$

[36]. Which gives $\beta = 4\%$ for for the DIII-D base case.

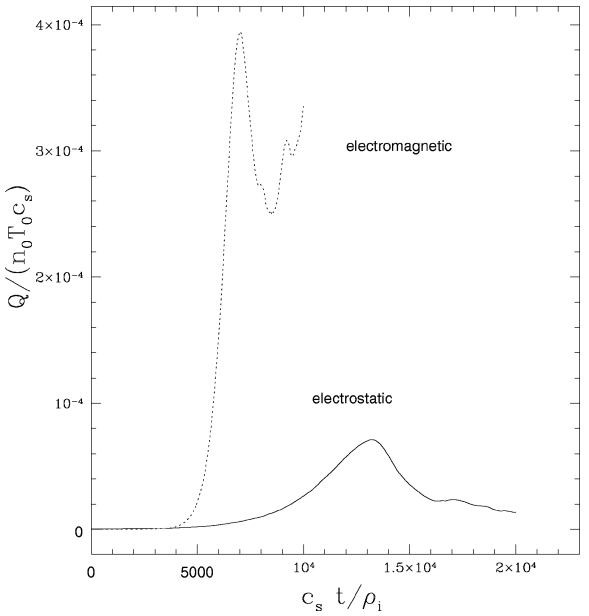

Fig. 4. Heat flux versus time for two cases: (1) electrostatic with $\beta = 0$ and (2) electromagnetic with $\beta = 3\%$. Parameters are from the DIII-D Cyclone base case. Heat flux is significantly higher for the $\beta = 3\%$ case.

To show presence of the shear Alfvén wave in a very simple way, assume a spatially uniform plasma and neglect the ion response, $\delta\bar{n}_\mathrm{i} = 0$, $J_{\|\mathrm{i}} = 0$. Linearizing Eqs. (7), (8), (10), (17) and (20), we obtain the following shear Alfvén dispersion relation

$$\omega^2 = k_\|^2 v_\mathrm{A}^2 \left(1 + k_\perp^2 \rho_s^2\right). \tag{21}$$

Eqs. (18) and (20) can be generalized to include collisional parallel resistivity and a Landau-fluid term to model collisionless dissipation [37]

$$E_\| = \eta_\mathrm{e} J_\| + \eta_\mathrm{Lf}(k_\|) J_{\|,\mathrm{e}} - \frac{1}{e n_\mathrm{e}} \tilde{\mathbf{b}} \cdot \nabla P_\|, \tag{22}$$

where

$$\eta_\mathrm{Lf}(k_\|) = \frac{\sqrt{\pi}}{2} \frac{|k_\|| v_{te}}{e^2 n_0},$$

and the η_e is the classical collisional electron resistivity.

We can include the effects from $\delta\mathbf{B}_\|$ by assuming perpendicular force balance is maintained and adding the appropriate terms to the ion gyrokinetic and drift-fluid electron equations. Perpendicular force balance gives

$$\mathbf{J}_\perp = -\frac{c}{B} \nabla_\perp \delta p_\perp \times \hat{\mathbf{b}}, \tag{23}$$

where $\delta p_\perp$ is the total pressure. Ampere's law then gives $\delta\mathbf{B}_\|$

$$\nabla^2 \mathbf{A}_\perp = -\frac{4\pi}{c} \mathbf{J}_\perp, \tag{24}$$

where $\delta\mathbf{B}_\| = \nabla \times \mathbf{A}_\perp$.

Assuming small β, $\delta B_\|$ is often neglected in Alfvénic drift-type turbulence calculations since $\delta B_\perp$ should play a more important role for cross-field transport. To motivate some justification for neglecting $\delta B_\|$ (as we have done

here as a simplifying first step), we estimate the order of magnitude of $\delta B_\parallel$ relative to $\delta B_\perp$. Using Eqs. (23)–(24) we obtain the following approximate relation

$$\frac{\delta B_\parallel}{B} \sim \frac{4\pi}{c} k_\perp \frac{A_\perp}{B} \sim 4\pi \frac{\delta p}{B^2} \sim \beta \frac{\delta p}{p}. \tag{25}$$

We can get a crude estimate of $\delta B_\perp$ by assuming $E_\parallel \approx 0$ which is the ideal MHD limit

$$\frac{\delta B_\perp}{B} \sim \frac{4\pi}{c} k_\perp \frac{A_\parallel}{B}, \tag{26}$$

$$E_\parallel \approx 0 = -\hat{\mathbf{b}} \cdot \nabla\phi - \frac{1}{c}\partial_t A_\parallel \Rightarrow k_\parallel \phi \sim \frac{\omega}{c} A_\parallel, \tag{27}$$

$$\Rightarrow \frac{\delta B_\perp}{B} \sim k_\perp \rho_s c_s \frac{k_\parallel}{\omega} \frac{e\phi}{T_\mathrm{e}}. \tag{28}$$

Next, we use the following approximate relation from the linearized ion pressure equation, $\delta P_k \sim \frac{\omega_{*T}}{\omega}\phi_k$, assuming $\eta_\mathrm{i} \gg 1$, to get an estimate of the ratio of $\delta B_\parallel$ to $\delta B_\perp$

$$\frac{\delta B_\parallel}{\delta B_\perp} \sim \beta \frac{\omega_{*T}}{k_\parallel c_s} \frac{1}{k_\perp \rho_s} \sim \beta \frac{qR}{L_T}. \tag{29}$$

Thus, $\delta B_\parallel$ should be small for Alfvénic ITG turbulence, assuming Eq. (27) can be used to relate ϕ and $A_\parallel$.

5. Transport reduction using temperature profile ripple

We have found a close relationship between the flux-surface-averaged (purely radial) perpendicular temperature $\langle \delta T_\perp \rangle$ and the flux-surface-averaged (purely radial) electrostatic potential $\langle \delta\phi \rangle$. This seems to be a general result in electrostatic flux-tube simulations. In Ref. [26], we obtained a simple relationship between these two quantities starting with a Hasegawa–Mima-type equation derived from the guiding center gyrofluid equations [24] for purely radial modes

$$\langle \delta\phi \rangle \approx -\frac{1}{2}\left(1 + \frac{\bar{k}_\perp^2}{k_\mathrm{r}^2}\right) \langle \delta T_\perp \rangle, \tag{30}$$

where k_r is the radial wave number of $\langle \delta\phi \rangle$ and $\bar{k}_\perp$ parameterizes the background turbulent fluctuations. This relation is observed in simulation (see, for example, Fig. 5) explains stationary purely radial modes in the situation where the there is strong profile variation (global simulations). The heat flux attempts to flatten the temperature profile generating a $\langle \delta T_\perp \rangle$. This nonlinearly generates $\langle \delta\phi \rangle$ from Eq. (30). For the case with no profile variation, or constant L_T (flux-tube simulations), the fluctuations in $\langle \delta T_\perp \rangle$ coming from fluctuations in the heat flux are turbulent. Note that this effect is *not* simply the balancing of E_r and ∇P in the radial force balance equation, but is a nonlinear generation of $\langle n \rangle$, which in turn generates E_r.

Using the relation between $\langle \delta\phi \rangle$ and $\langle \delta T_\perp \rangle$, we have shown that slight ripple ($\sim$5%) or small bumps to the equilibrium temperature profile on the scale of $\sim 30\rho_\mathrm{i}$ enhance the self-generated shear flows thereby reducing turbulent transport [26]. Previously, we did *not* include the important effect of equilibrium E_r shear [5–9] in test simulations. The radial force balance is

$$E_\mathrm{r} = \frac{1}{en_\mathrm{i}} \frac{\mathrm{d}P_\mathrm{i}}{\mathrm{d}r} + u_\phi B_\theta - u_\theta B_\phi. \tag{31}$$

Therefore, the ripple in the temperature may cause a ripple in the equilibrium E_r. Assuming, there is no fluid flow, there will be a ripple in the equilibrium potential from the temperature ripple.

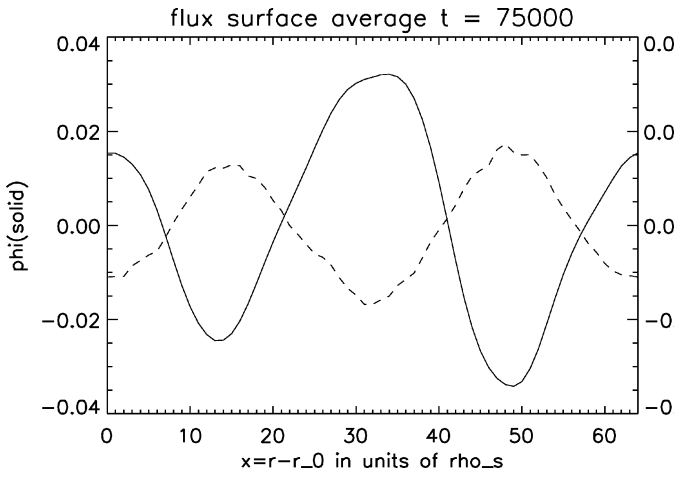

Fig. 5. Weak, short-scale sinusoidal variation of the temperature profile reduces the heat flux. $T_{\rm eq}(r) \approx T_0(r)(1 + 0.02\cos(0.2\frac{r}{\rho_{\rm i}}))$ (a) flux-surface average electrostatic potential $\langle\delta\phi\rangle(x)$, and (b) perpendicular ion pressure $\langle P_\perp\rangle(x)$ versus $x = r - r_0$. Parameters are from the DIII-D Cyclone base case.

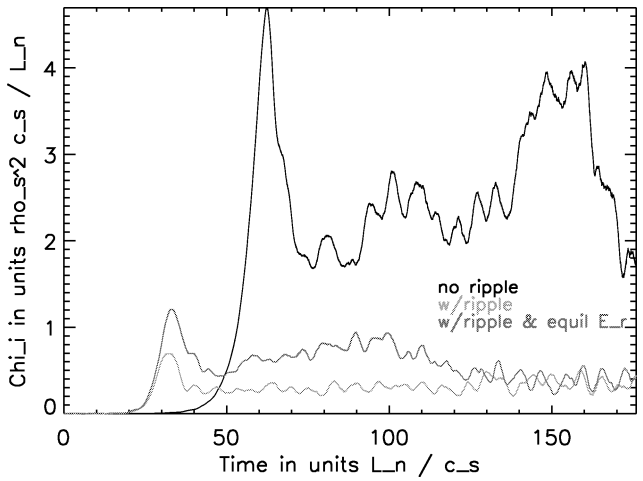

Fig. 6. Heat flux versus time with and without equilibrium temperature profile ripple. Two cases with temperature profile ripple are shown, one with the effect of equilibrium $E_{\rm r}$ shear and the other without it. Parameters are from the DIII-D Cyclone base case.

From Eq. (31), $\delta\phi_{\rm eq} = -\delta T_{\rm eq}$. Hence, the nonlinearly generated $\langle\delta\phi\rangle$ from Eq. (30) may cancel the equilibrium $E_{\rm r}$. The new result here, is that we now include the equilibrium radial electric field coming from Eq. (31) and still find a significant reduction in transport from the temperature profile ripple (Fig. 6).

In the simulation, we approximate the equilibrium temperature profile ripple in the following way

$$T_{\rm eq}(r) = T_0(r)\big[1 + \epsilon\cos(k_0 x)\big]. \tag{32}$$

The corresponding temperature gradient or drive of the instability is

$$L_T^{-1} = -\frac{1}{T}\frac{{\rm d}T}{{\rm d}r} \approx \frac{1}{T_0}\frac{{\rm d}T_0}{{\rm d}r} - \epsilon k_0\sin(kx), \tag{33}$$

$$= L_{T0}^{-1}\big[1 - \epsilon k_0 L_{T0}\sin(k_0 x)\big]. \tag{34}$$

This variation of the drive causes stationary spatial oscillations in the flux and hence $\langle T_\perp \rangle(x)$, which in turn nonlinearly generates E_r shear, that suppresses the turbulent transport.

Fig. 5 shows $\langle \delta\phi \rangle$ and $\langle \delta P_\perp \rangle$ from a flux-tube simulation with a 34% variation in L_T^{-1}, which corresponds to only a 2% temperature ripple with typical H-mode parameters. In the simulation, it is easier to measure $\langle P_\perp \rangle = \langle \int \frac{v_\perp^2}{2} \delta f \mathrm{d}^3 v \rangle$ rather than $\langle T_\perp \rangle$. Simulation results show that $\langle n \rangle \ll \langle T_\perp \rangle$, which is consistent with theoretical expectations [26], so we assume $\langle T_\perp \rangle \approx \langle P_\perp \rangle$.

The DIII-D base case parameters described in Section 3 were used along with: 8 particles per cell, $128 \times 128 \times 32$ grid, with $\Delta x = \Delta y = \rho_s$, and a time step of $\Delta t c_s / L_T = 0.037$. Fig. 4 shows the heat flux versus time for three cases. The first case has no temperature profile ripple. The second case has temperature profile ripple, but *no* equilibrium E_r. The third case includes both the ripple as well as the self-consistent equilibrium E_r from radial force balance equation (32). This is the most important case, since it shows that the ripple reduces the heat transport and that the self-generated purely radial E_r does *not* simply cancel the equilibrium E_r.

There is still an open question of whether it is practical to actually generate a small and relatively short scale temperature profile variation from flux-surface to flux-surface. More work is needed to study feasibility with (1D diffusion) transport models. It may be possible to ripple the temperature profile using ion-cyclotron resonance heating with multiple RF sources or variable frequency. This would rely on some focusing of the launched wave toward the vertical center of the plasma. Not restricting our discussion to present-day RF systems, one plausible scheme would be to frequency modulate the RF heating carrier frequency with a stair-case waveform, causing a slight heating of flux-surfaces spaced $\sim 30\rho_\mathrm{i}$ apart.

6. Summary

We described a drift-fluid-electron hybrid model which is used to obtain the electron parallel current. This is used to study electromagnetic Alfvénic ITG turbulence in gyrokinetic simulation. Initial results are shown using nonlinear gyrokinetic ions and linearized drift-fluid electrons in three-dimensional toroidal geometry. Large values of $\beta \gtrsim 1.5\%$ show strong destabilization relative to the electrostatic limit. Nonlinear simulations show an enhanced heat flux as well.

Second, very good parallel performance and near perfect scalability is shown on the Cray T3E and SGI O2K using a one-dimensional domain decomposition and digital filtering to handle the shifts at the boundaries along the magnetic field-line due to toroidal boundary conditions when using field-aligned coordinates.

Finally, we discussed the fact that the self-generated E_r is closely related to $\langle \delta T_\perp \rangle$ and how a small $\sim 2\%$ equilibrium temperature profile ripple on the scale of $\sim 30\rho_\mathrm{i}$ significantly reduces heat transport in electrostatic ITG turbulence simulations. The important effect of the equilibrium E_r from radial force balance was included in these calculations for the first time. The feasibility of using ion-cyclotron resonance heating or some other mechanism to to ripple the temperature needs to be explored further.

Acknowledgments

We give special thanks to all the members of the “Cyclone Team”, as well as L. Chen, V. Decyk and P. Snyder. This research is supported by U.S. Department of Energy (DOE) Grant No. DE-FG03-97ER5442(4/6). This work is an active part of the Numerical Tokamak Turbulence Project DOE Grand Challenge. Computing resources where generously provided by the Advanced Computing Laboratory at Los Alamos National Laboratory, the National Energy Research Scientific Computing Center at Lawrence Berkeley National Laboratory.

References

[1] S. Parker, W. Lee, R. Santoro, Phys. Rev. Lett. 71 (1993) 2042.
[2] A. Dimits, T. Williams, J. Byers, B. Cohen, Phys. Rev. Lett. 77 (1996) 71.
[3] R. Sydora, V. Decyk, J. Dawson, Plasma Phys. Controlled Fusion 38 (1996) A281.
[4] Z. Lin, T. Hahm, W. Lee, W. Tang, R. White, Science 281 (1998) 1835.
[5] H. Biglari, P. Diamond, P. Terry, Phys. Fluids B 2 (1990) 1.
[6] P. Diamond, Y. Kim, Phys. Fluids B 3 (1991) 1626.
[7] S. Hamaguchi, W. Horton, Phys. Fluids B 4 (1992) 319.
[8] T. Hahm, K.H. Burrell, Phys. Plasmas 2 (1995) 1648.
[9] R. Waltz, G. Kerbel, J. Milovich, Phys. Plasmas 1 (1994) 2229.
[10] J.V.W. Reynders, Ph.D. Thesis, Princeton University (1992).
[11] J.C. Cummings, Ph.D. Thesis, Princeton University (1994).
[12] B. Cohen, A. Dimits, Phys. Rev. E 56 (1997) 2151.
[13] H. Naitou, K. Hironori, S. Tokuda, J. Plasma Fusion Res. 73 (1997) 174.
[14] P. Snyder, Ph.D. Thesis, Princeton University (1999).
[15] P. Snyder, G. Hammet, M. Beer, W. Dorland, Bull. Amer. Phys. Soc. 44 (1999) 1013.
[16] E. Frieman, L. Chen, Phys. Fluids 25 (1982) 502.
[17] W. Lee, Phys. Fluids 26 (1983) 556.
[18] D. Dubin, J. Krommes, C. Oberman, W. Lee, Phys. Fluids 26 (1983) 3524.
[19] T.S. Hahm, Phys. Fluids 31 (1988) 2670.
[20] A.J. Brizard, J. Plasma Phys. 41 (1989) 541.
[21] This list of papers may not be complete and includes only the later work on nonlinear gyrokinetics, please check references within.
[22] S. Parker, W. Lee, Phys. Fluids B 5 (1993) 77.
[23] W.W. Lee, J. Comput. Phys. 72 (1987) 243.
[24] W. Dorland, G. Hammett, Phys. Fluids B 5 (1993) 812.
[25] M. Beer, S. Cowley, G. Hammett, Phys. Plasmas 2 (1995) 2686.
[26] S. Parker, C. Kim, Y. Chen, Phys. Plasmas 6 (1999) (to appear).
[27] S. Cowley, R. Kulsrud, R. Sudan, Phys. Fluids B 13 (1991) 2767.
[28] R.B. White, M.S. Chance, Phys. Fluids 27 (1984) 2455.
[29] V. Decyk, Comput. Phys. Commun. 87 (1995) 87.
[30] T. Williams, Proceedings High Performance Computing: Grand Challenges for Compiter Simulation, March 29, Arlington, VA (1995).
[31] J. Byers et al., J. Comput. Phys. 27 (1978) 363.
[32] D.E. Hewett, J. Comput. Phys. 38 (1980) 378.
[33] D. Harned, J. Comput. Phys. 47 (1982) 452.
[34] S. Parker, H. Mynick, M. Artun, V. Decyk, J. Kepner, W. Lee, W. Tang, Phys. Plasmas 3 (1996) 1461.
[35] Y. Chen, S.E. Parker, Bull. Amer. Phys. Soc. 44 (1999) 357.
[36] J. Freidberg, Rev. Mod. Phys. 54 (1982) 801.
[37] G. Hammett, F. Perkins, Phys. Rev. Lett. 64 (1990) 3019.